ELSEVIER

Journal of Nuclear Materials 279 (2000) 100–106

journal of nuclear materials

www.elsevier.nl/locate/jnucmat

Crystallization sequence and microstructure evolution of Synroc samples crystallized from $CaZrTi_2O_7$ melts

Huifang Xu [a,*], Yifeng Wang [b]

[a] *Transmission Electron Microscopy Laboratory, Department of Earth and Planetary Sciences, The University of New Mexico, Albuquerque, NM 87131-1116, USA*

[b] *Sandia National Laboratories, 115 North Main Street, Carlsbad, NM 88220, USA*

Received 21 May 1999; accepted 1 November 1999

Abstract

Scanning electron microscopy (SEM), high-resolution transmission electron microscopy (HRTEM) and analytical electron microscopy (AEM) studies have been conducted on samples crystallized from melts with a composition of zirconolite $\{(Ca_{0.9}Gd_{0.1})Zr(Ti_{1.9}Al_{0.1})_2O_7\}$. The formation of a whole suite of Synroc phases (zirconia, $ZrTiO_4$, zirconolite, perovskite and rutile) has been observed. In the $CaZrTi_2O_7$ system, the formation of these phases follows the crystallization sequence of Ti-bearing zirconia → $ZrTiO_4$ phase → Zr-rich zirconolite → Zr-poor zirconolite → rutile/perovskite. This sequence is induced by a fractional crystallization process, in which Zr-rich phases tend to crystallize first, resulting in continuous depletion of Zr in melt. Consistent with this melt compositional evolution, the Zr content in the zirconolite decreases from the area next to the $ZrTiO_4$ phase to areas next to rutile or perovskite. High-resolution TEM images show that there are no glassy phases at the grain boundary between zirconolite and perovskite. The fractional crystallization-induced textural heterogeneity may have a significant impact on the incorporation of radionuclides into crystalline phases and the resistance of radionuclides to leaching processes. Exsolution lamellae and multiple twinning resulting from the phase transition from tetragonal zirconia to monoclinic zirconia may decrease durability of the Synroc. Fast cooling of the melt may produce more zirconolite phase and relatively uniform texture. In general, however, a Synroc prepared by melting is less uniform in texture than that prepared by a sol–gel method.

PACS: 61.14.-x; 61.16.Bg; 81.10.Fq; 81.30.-t; 81.30.Hd

1. Introduction

Development of highly durable waste forms is the key to permanent disposal of HLW, including surplus weapons-usable plutonium in geologic repositories. Synroc is a durable titanate ceramic waste form with zirconolite ($CaZrTi_2O_7$), pyrochlore ($Ca(U,Pu)Ti_2O_7$), perovskite ($CaTiO_3$), hollandite as major crystalline phases and has been shown to be particularly promising for immobilizing various high level wastes [1–12]. The concept of Synroc was originally proposed by Ringwood et al. and the first Synroc fabrication technology was developed by Dosch et al. [1]. During the last two decades, Synroc has been subjected to extensive studies [1–14]. Synroc immobilizes radionuclides by incorporating them into appropriate phases and forming solid solutions. With large polyhedra (with coordination numbers ranging from 7 to 12) in the structures, Synroc is able to accommodate a wide range of radionuclides (e.g., actinides, Pu, U, Ba, Sr, Cs, Rb, Tc, etc.) as well as neutron poisons (e.g., Gd) [10]. U- and Pu-loaded Synroc generally contains phases of pyrochlore and zirconolite, a derivative structure of pyrochlore [1–3,7,8,15]. The pyrochlore phase can incorporate more Pu than the

* Corresponding author. Tel.: +1-505 277 7536; fax: +1-505 277 8843.

E-mail addresses: hfxu@unm.edu (H. Xu), ywang@nwer.sandia.gov (Y. Wang).

0022-3115/00/$ - see front matter
PII: S0022-3115(99)00272-X

zirconolite phase [3]. Various Synroc formulations (e.g., Synroc-C, Synroc-D, Synroc-E, Synroc-F etc.) have been developed for specific HLWs [1,15–17]. Limited number of comparative corrosion tests have indicated that Synroc may be more durable than many types of borosilicate glass waste forms [1,2,14].

As well as pressing and sintering, Synroc waste forms can be prepared by either a sol–gel method or a melting method. The Synroc prepared by the sol–gel method is usually fine-grained and relatively uniform compared to that produced from a melt. Textural heterogeneity in the Synroc can directly impact the incorporation of radionuclides into crystalline phases and the corrosion resistance. In this paper, we study the phases and microstructure evolution of a with zirconolite ($CaZrTi_2O_7$) dominated Synroc crystallized from a melt.

2. Samples and experiments

A powder mixture with a stoichiometric composition of Gd-bearing zirconolite, $(Ca_{0.9}Gd_{0.1})Zr(Ti_{1.9}Al_{0.1})_2O_7$, was prepared by mixing different oxides. The mixture was placed in corundum crucibles and melted at 1600°C. One set of melts was quenched to room temperature and then annealed at 900°C for 10 h. The other set of melts was cooled down to room temperature at the rate of ~100°C and 50°C per h, respectively. Double-side polished petrographic thin sections were prepared for SEM and TEM investigations. The samples for TEM studies were selected from the thin sections and then ion milled. All high resolution transmission electron microscopy (HRTEM) and AEM EDS results were carried out with a JEOL 2010 HRTEM and Oxford Link ISIS EDS system. Point-to-point resolution of the HRTEM is 0.19 nm. Mineral standards of anorthite (for k_{Ca} and k_{Al}), zircon (for k_{Zr}) and sphene (for k_{Ti}) were used for quantification of collected EDS data (see Appendix A for detail). We used a theoretical k_{Gd} value, because no standard was available for Gd.

3. SEM results

Backscattered electron images (Fig. 1) show heterogeneous textures of ceramic samples crystallized from a zirconolite ($CaZrTi_2O_7$) melt. The samples contain a whole suite of Synroc phases zirconolite, perovskite, rutile and $ZrTiO_4$ phase. A minor amount of Al_2TiO_5 phase may come from the crucible during sample preparation. The fast cooled sample displays more uniform texture and less $ZrTiO_4$ core than the quenched and slowly cooled samples.

The fast cooled samples display a typical phase zonation with $ZrTiO_4$ as cores surrounded by zirconolite, which is in turn enclosed by rutile and perovskite (Fig. 1). A slowly cooled sample shows zirconia cores surrounded by $ZrTiO_4$ phase, which is in turn enclosed by zirconolite (Fig. 1 left). A previous study on the crystallization of a similar composition melt at a relatively slow cooling rate (40°C/h) shows Ti-bearing zirconia cores were formed and surrounded by zirconolite rims [18]. The zirconia

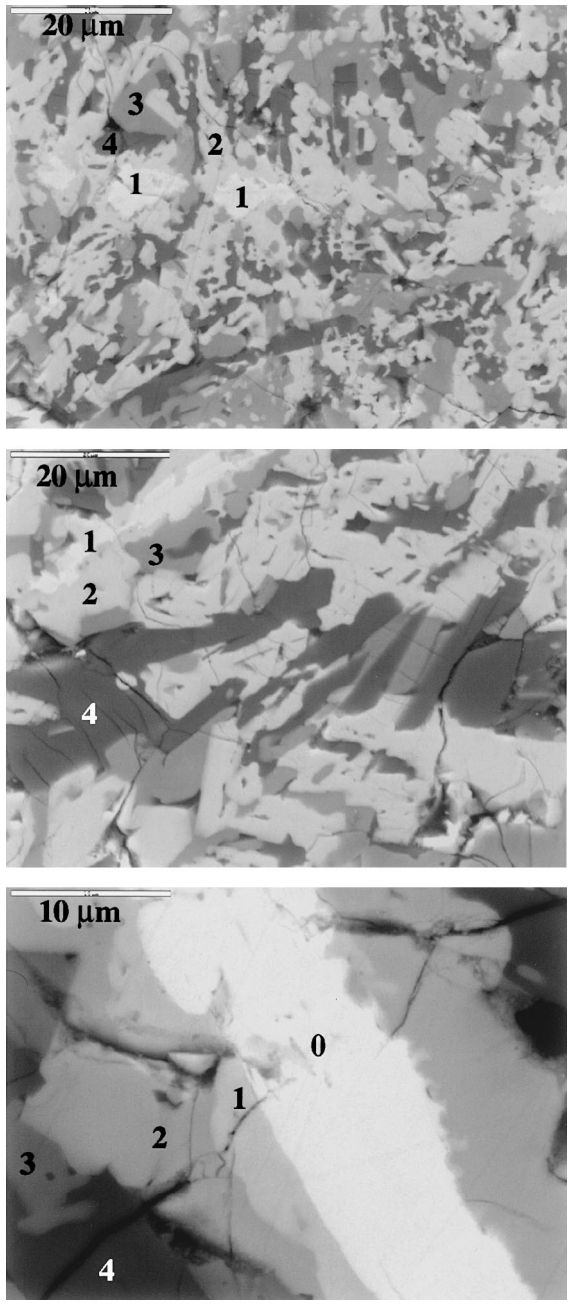

Fig. 1. Backscattered electron images of the slowly cooled (bottom), fast cooled (center), and quenched (top) samples showing zirconia core (0), $ZrTiO_4$ core (1), zirconolite (2), rutile (3) and perovskite (4).

may contain 15 mol% of TiO_2 [18]. Based on our experimental results, we suggest that there should be a zone of $ZrTiO_4$ between the zirconia core and zirconolite rim. The zone might have been mis-identified as zirconia too. The phases formation sequence can be expressed as a fractional crystallization process:

$$CaZrTi_2O_7(\text{melt}) \rightarrow xZrO_2 + CaZr_{1-x}Ti_2O_{7-2x}(\text{melt})$$

$$CaZr_{1-x}Ti_2O_{7-2x}(\text{melt}) \rightarrow yZrTiO_4 + CaZr_{1-x-y}Ti_{2-y}O_{7-2x-4y}(\text{melt})$$

$$CaZr_{1-x-y}Ti_{2-y}O_{7-2x-4y}(\text{melt}) \rightarrow zCaZrTi_2O_7 + Ca_{1-z}Zr_{1-x-y-z}Ti_{2-y-2z}O_{7-2x-4y-7z}(\text{melt})$$

$$Ca_{1-z}Zr_{1-x-y-z}Ti_{2-y-2z}O_{7-2x-4y-7z}(\text{melt}) \rightarrow (1-x-y-z)CaZrTi_2O_7 + (x+y)CaTiO_3 + xTiO_2$$

During the fractional crystallization, Zr-rich phases tend to crystallize first, resulting in continuous depletion of Zr in the melt and the formation of rutile and perovskite as final crystallization products.

4. TEM and AEM results

The Ti-bearing zirconia cores in a slowly cooled sample display twinning and exsolution lamellae (Fig. 2). The twinning is resulted from a martensitic phase transformation from cubic and tetragonal symmetry to monoclinic symmetry. The exsolution lamellae with periodic distribution are similar to those resulting from spinodal decomposition. The Zr-poor lamellae may be $ZrTiO_4$ phase or Zr-bearing rutile. Consistent with the melt compositional evolution during the fractional crystallization, the $ZrTiO_4$ phase displays a systematical compositional change away from the $ZrTiO_4$–zirconolite interface: $Zr_{1.89}Ti_{2.01}Ca_{0.06}Al_{0.06}O_8 \rightarrow Zr_{2.09}Ti_{1.83}Ca_{0.03}Al_{0.08}O_8 \rightarrow Zr_{2.16}Ti_{1.81}Ca_{0.05}Al_{0.02}O_8$. A weak exsolution lamellae-like feature is visible in the crystal, which may indicate possible exsolution between ordered $ZrTiO_4$ and $ZrTi_2O_6$ at low temperature [21] (Fig. 3(a)). Similarly, the content of Zr in zirconolite decreases from the $ZrTiO_4$-zirconolite interface ($Ca_{0.79}Zr_{1.20}Gd_{0.12}Ti_{1.55}Al_{0.36}O_7$) to the zirconolite-rutile interface ($Ca_{1.00}Zr_{0.65}Gd_{0.08}Ti_{2.18}Al_{0.14}O_7$) (Table 1). The Zr-rich zirconolite results from the reaction between the early formed $ZrTiO_4$ phase and the melt. The Zr-poor zirconolite is a crystallization product of the remaining melt. The zirconolite crystals contain dense (0 0 1) stacking faults with stacking vectors of $(\mathbf{a}/4 + \mathbf{c}/2)$ and $(\mathbf{b}/4 + \mathbf{c}/2)$, respectively (Fig. 2). SAED patterns show streaking reflections along the $\mathbf{c}^*$ direction except the $(h\,k\,l)$ reflections with $(h/4 + k/4 + l/2 = \text{integers})$. In the areas with dense stacking faults, there are nonperiodic stacking of domains of 2-layer and 3-layer zirconolite polytypes (Fig. 3(b)) that was described in references [22,23]. In the areas with dense stacking faults, pyrochlore-like lamellae occur within the zirconolite (Fig. 3(b)). HRTEM image also shows the boundary between the coexisting zirconolite and perovskite is

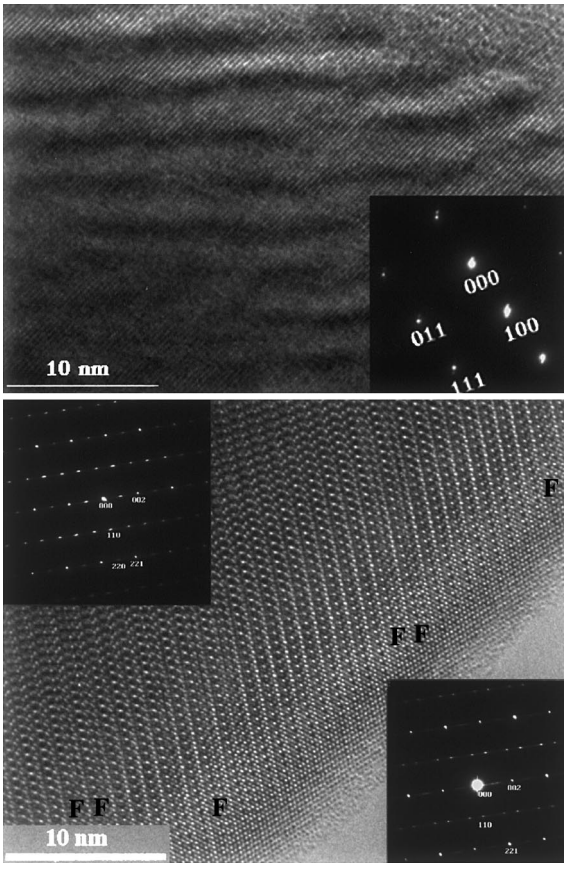

Fig. 2. HRTEM images showing exsolution lamellae in the Ti-bearing zirconia (upper) and stacking faults (F) in a 2-layer polytype zirconolite (lower). Inserted SAD patterns are from the areas containing low density of the faults (upper-left corner) and high density of the faults (lower-right corner), respectively.

Table 1
Compositional changes of zirconolite from zirconolite/$ZrTiO_4$ interface (point 1) to zirconolite/rutile interface (point 7)

1.	$Ca_{0.79}Zr_{1.20}Gd_{0.12}Ti_{1.55}Al_{0.36}O_7$
2.	$Ca_{0.70}Zr_{1.18}Gd_{0.12}Ti_{1.58}Al_{0.40}O_7$
3.	$Ca_{0.78}Zr_{1.17}Gd_{0.15}Ti_{1.59}Al_{0.33}O_7$
4.	$Ca_{0.81}Zr_{1.15}Gd_{0.12}Ti_{1.58}Al_{0.36}O_7$
5.	$Ca_{0.94}Zr_{0.94}Gd_{0.06}Ti_{1.88}Al_{0.23}O_7$
6.	$Ca_{0.88}Zr_{0.93}Gd_{0.07}Ti_{1.93}Al_{0.21}O_7$
7.	$Ca_{1.00}Zr_{0.65}Gd_{0.08}Ti_{2.18}Al_{0.14}O_7$

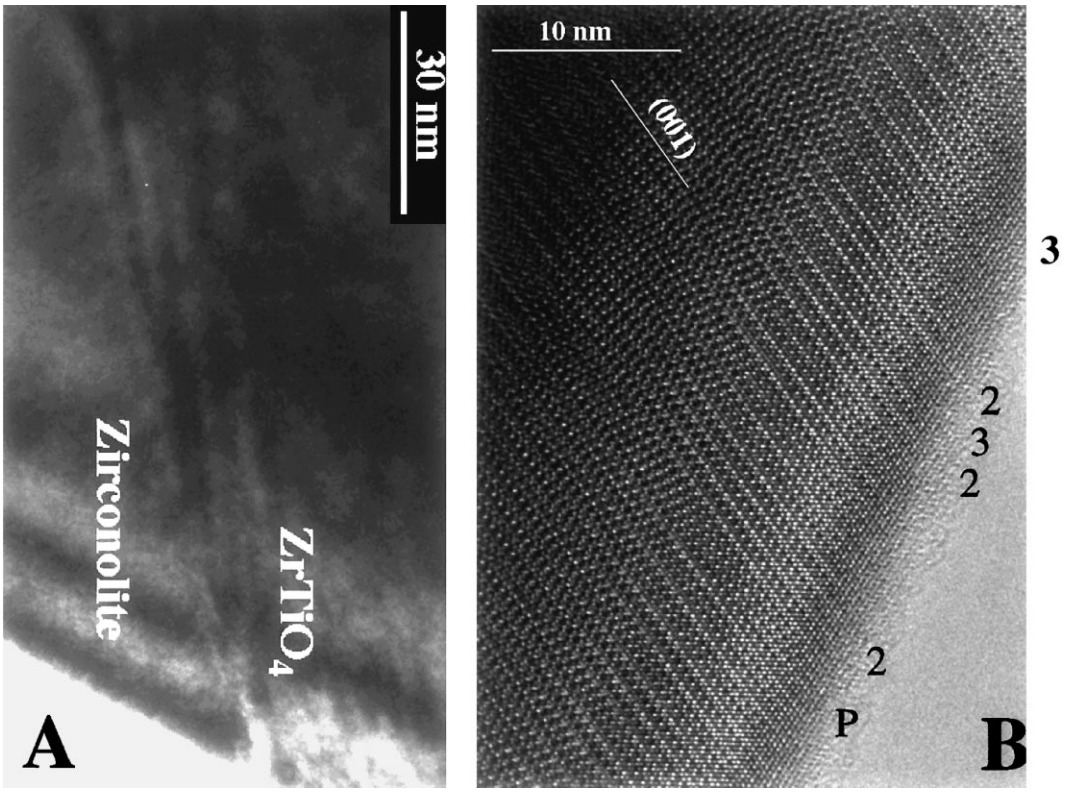

Fig. 3. (A) TEM images showing an interface between zirconolite and the ZrTiO4 phase. There are exsolution lamellae in the ZrTiO4 phase. (B) HRTEM image of the zirconolite showing domains of 2-layer and 3-layer zirconolite polytypes and a pyrochlore-like domain (P).

bonded; that is, oxygen atoms at the boundaries are shared by the co-existing phases (Fig. 4). No glassy phases exist at the grain boundaries. The most Zr-rich rutile at the zirconolite-rutile interface is $Ti_{0.95}Zr_{0.04}Al_{0.01}Ca_{0.01}O_2$. The composition of the perovskite is $Ca_{0.94}Ti_{1.01}Zr_{0.02}O_7$.

5. Fractional crystallization of the melt

Based on the observed textural and compositional results from TEM and AEM study, it can be inferred that crystallization of the $CaZrTi_2O_7$ melt is a process of fractional crystallization that is similar to the crystallization of silicate magma system, such as the system of pyroxene [19]. The crystallization sequence is: Ti-bearing zirconia, $ZrTiO_4$ phase, Zr-rich zirconolite, Zr-poor zirconolite and rutile/perovskite. The crystallization of the melt can be expressed as a pseudo-binary system with two peritectic points and one eutectic point (Fig. 5). Zirconia crystallizes first from the melt. As a result, Zr content in the melt decreases and Ti content in the zirconia increases. As the temperature reaches the first peritectic point (2), the early formed zirconia reacts with the melt and forms a $ZrTiO_4$ phase as rims surrounding the zirconia. After the temperature passes the peritectic point (2), the Ti-rich $ZrTiO_4$ phase crystallizes from the melt. As the temperature reaches the second peritectic point (3), the early-formed $ZrTiO_4$ phase reacts with the melt and forms Zr-rich zirconolite as rims surrounding the zirconia. As the temperature decreases further and passes the second peritectic point (3), the Zr-poor zirconolite crystallizes from the melt. As the temperature decrease further and reaches the (pseudo-) eutectic point, the Zr-poor zirconolite co-crystallizes with rutile and perovskite. Further cooling of the crystals results in the formation of multiple twinning and Ti-rich exosultion lamellae in the Ti-bearing zirconia and exsolution in the $ZrTiO_4$ phase (sub-solidus reaction). Exsolution lamellae and multiple twinning resulting from the phase transition from tetragonal zirconia to monoclinic zirconia may decreases the durability of Synroc. If the crystallization were under an equilibrium condition, the $ZrTiO_4$ phase would react with the melt completely and the final product would be zirconolite only. In reality, however, the remaining melt is unlikely to react with the

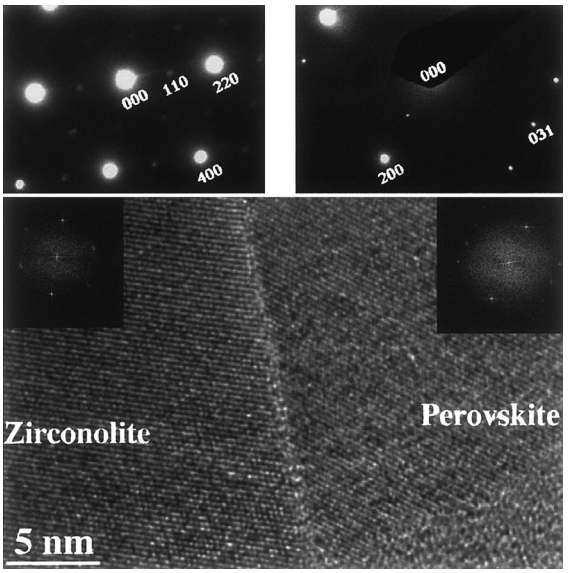

Fig. 4. SAED patterns (upper) and HRTEM image (lower) of zirconolite (left) and perovskite (right) from the Synroc sample. The zirconolite and perovskite bond (or connect) each other across the grain boundary. Diffractograms from the areas of zirconolite and perovskite across the boundary are also inserted at the upper corners of the HRTEM image.

early-formed phases completely and a fractional crystallization often occurs. Thus, the Synroc prepared by the melting is generally less uniform in texture than that prepared by the sol–gel method. The sample prepared at a fast cooling rate (e.g., 100°C/h) seems to produce more zirconolite phase and more uniform texture than the samples prepared at a low cooling rate (e.g., 50°C/h). It is proposed that crystallization sequence of $CaPuTi_2O_7$ system is similar to that of $CaZrTi_2O_7$ system [20]. The difference will be no $TiPuO_4$ intermediate phase in the

Table 2
K-factors for the UNM JEOL 2010 HRTEM[a]

Element ratio	Standard	*K*-factor (K_{x-Si})
Na/Si	Albite	1.44
	Jadeite	1.36
Mg/Si	Enstatite	1.19
Al/Si	Anorthite	1.02
	Jadeite	1.00
K/Si	K-feldspar	0.94
Ca/Si	Anorthite	0.95
Ti/Si	Titanite	1.25
Mn/Si	Rhodonite	1.22
Fe/Si	Fayalite	1.25
Co/Si	Co-olivine	1.39
Ni/Si	Ni-olivine	1.30
Cu/Si	Shattuckite	1.48
Zn/Si	Willemite	1.51
Zr/Si[b]	Zircon	1.79
Re/Si[c]	$KReO_4$	1.93

[a] Condition: X-tilt = +10°, Y-title = 0°, Spot size = 2 (EDS mode).
[b] Use L_α line.
[c] Use *M* line.

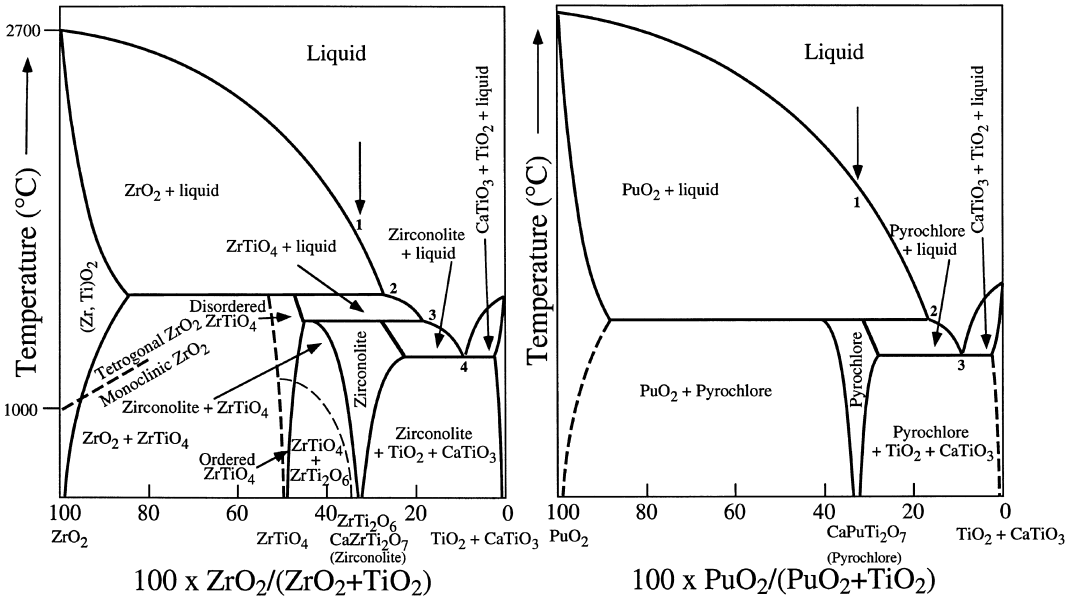

Fig. 5. A proposed phase diagram topology for the pseudo-binary systems of ZrO_2–$(TiO_2 + CaTiO_3)$ (left) and PuO_2–$(TiO_2 + CaTiO_3)$ (right), respectively.

system of PuO_2–($TiO_2 + CaTiO_3$) because of large difference in ionic radii between Zr (0.079 nm) and Pu (0.093 nm). A phase diagram topology for the system of PuO_2–($TiO_2 + CaTiO_3$) is also proposed (Fig. 5).

Acknowledgements

This work is based upon research conducted at the Transmission Electron Microscopy Laboratory in the Department of Earth and Planetary Sciences of the University of New Mexico, which is partially supported by NSF, NASA and State of New Mexico. Authors also thank anonymous reviewers who provided critical comments.

Appendix A. Analytical electron microscope standardization

Both natural and synthetic minerals were used as standards and were chosen on the basis of their chemical homogeneity, simplicity of composition and relative stability under electron beam. AEM EDS analyses were carried out in a JEOL 2010 HRTEM with an attached Oxford Link ISIS EDS system and a Li-drifted Si detector with ultrathin window. Accelerating voltage is 200 keV. All specimens were tilted 10° towards the detector (X-tilt = 10°) to minimize continuum-fluoresced X-ray while maximizing peak intensities. Zone-axis oriented crystal grains were not used for data collection, in order to avoid channeling effect. The peak intensities (L_α for Zr and K_α for other elements) were used in the Cliff–Lorimer thin film ratio equation [24]. This method is valid when the effects of absorption and fluorescence are negligible, which requires very thin areas of analyzed samples. The condition is critical for compounds containing heavy elements such as Fe. In general, if oxygen peak is strong, the area of the analyzed oxides or oxygen-based compounds is suitable for EDS data collection. *K*-factors obtained in this study are listed in Table 2. The errors of AEM analyses under optimum condition are generally within 6%.

References

[1] R.G. Dosch, T.J. Headley, C.J. Northrup, P.F. Hlava, Sandia National Laboratories Report, Sandia 82-2980, 1982, p. 84.
[2] A.E. Ringwood, S.E. Kesson, K.D. Reeve, D.M. Levins, E.J. Ramm, Synroc., in: W. Lutze, R.C. Ewing (Eds.), Radioactive Waste Forms for the Future, North-Holland, Amsterdam, 1988, p. 233.
[3] A. Jostsons, E.R. Vance, D.J. Mercer, V.M. Oversby, in: T. Murakami, R.C. Ewing (Eds.), Scientific Basis for Nuclear Waste Management XVIII, Materials Research Society, Pittsburgh, 1995, p. 775.
[4] R.C. Ewing, W.J. Weber, W. Lutze, in: E.R. Merz, C.E. Walter (Eds.), Disposal of Excess Weapons Plutonium as Waste, NATO ASI Series, Kluwer Academic, Dordrecht, 1996, p. 65.
[5] W.J. Weber, R.C. Ewing, W. Lutze, in: W.M. Murphy, D.A. Knecht (Eds.), Scientific Basis for Nuclear Waste Management XIX, Materials Research Society, Pittsburgh, 1996, p. 25.
[6] A.J. Bakel, E.C. Buck, B. Ebbinghaus, in: Plutonium Future – The Science, Los Alamos National Laboratories, 1997, p. 135.
[7] B.D. Begg, E.R. Vance, in: W.J. Gray, I.R. Triay (Eds.), Scientific Basis for Nuclear Waste Management XX, Materials Research Society, Pittsburgh, 1997, p. 333.
[8] B.D. Begg, E.R. Vance, R.A. Day, M. Hambley, S.D. Conradson, in: W.J. Gray, I.R. Triay (Eds.), Scientific Basis for Nuclear Waste Management XX, Materials Research Society, Pittsburgh, 1997, p. 325.
[9] E.C. Buck, B. Ebbinghaus A.J. Bakel, J.K. Bates, in: W.J. Gray, I.R. Triay (Eds.), Scientific Basis for Nuclear Waste Management XX, Materials Research Society, Pittsburgh, 1997, p. 1259.
[10] E.R. Vance, MRS Bulletin XIX (1994) 28.
[11] E.R. Vance, A. Jostsons, M.W.A. Stewart, R.A. Day, B.D. Begg, M.J. Hambley, K.P. Hart, B.B. Ebbinghaus, in: Plutonium Future – The Science, Los Alamos National Laboratories, 1997a, p. 19.
[12] E.R. Vance, K.P. Hart, R.A. Day, M.L. Carter, M. Hambley, M.G. Blackford, B.D. Begg, in: W.J. Gray, I.R. Triay (Eds.), Scientific Basis for Nuclear Waste Management XX, Materials Research Society, Pittsburgh, 1997b, p. 341.
[13] G.R. Lumpkin, K.L. Smith, G. Mark, M.G. Blackford, in: T. Murakami, R.C. Ewing (Eds.), Scientific Basis for Nuclear Waste Management XVIII, Materials Research Society, Pittsburgh, 1995, p. 885.
[14] J.K. Bates, E.C. Buck, N.L. Dietz, T. DiSanto, W.L. Ebert, J.W. Emery, J.A. Fortner, L.D. Hafenrichter, J.C. Hoh, J.S. Luo, L. Nunez, M.T. Surchik, S.F. Wolf, D. Wronkiewicz, ANL technical support program for DOE office of Environmental Management annual report (ANL-96/11), Argonne National Laboratory, Argonne, IL, 1996, p. 140.
[15] A.G. Solomah, T.S. Sridhar, S.C. Jones, in: Advances in Ceramics, Nuclear Waste Management II, American Ceramic Society, vol. 20, Columbus, 1996, p. 259.
[16] L.L. Hench, D.E. Clarke, J. Campbell, Chemical Waste Management 5 (1984) 149.
[17] S.E. Kesson, A.E. Ringwood, in: G.L. McVay (Ed.), Scientific Basis for Nuclear Waste Management VII, Materials Research Society, Pittsburgh, 1984, p. 507.
[18] O.A. Knyazev, S.V. Stefanovsky, S.V. Ioudintsev, B.S. Nikonov, B.I. Omelianenko, A.V. Mokhov, A.I. Yakushev, in: W.J. Gray, I.R. Triay (Eds.), Scientific Basis for Nuclear Waste Management XX, Materials Research Society, Pittsburgh, 1997, p. 401.
[19] J.S. Huebner, Rev. Mineral. 7 (1980) 213.
[20] D. Swenson, T.G. Nieh, J.H. Fournelle, in: W.M. Murphy, D.A. Knecht (Eds.), Scientific Basis for Nuclear Waste Management XIV, Materials Research Society, Pittsburgh, 1996, p. 337.

[21] L.W. Coughanour, R.S. Roth, S. Marzullo, F.E. Sennett, J. Res. National Bureau of Standards 54 (1995) 191.
[22] T.J. White, Am. Mineral. 69 (1984) 1156.
[23] P. Bayliss, F. Mazzi, R. Munno, T.J. White, Mineral. Mag. 53 (1989) 565.
[24] G. Cliff, G.W. Lorimer, J. Microsc. 103 (1975) 203.